

# Observing ballistic transport beyond the mean free time

George Datsaris,\* Theo Geisel, and Ragnar Fleischmann

Max Planck Institute for Dynamics and Self-Organization

(Dated: Friday 4<sup>th</sup> April, 2025)

Characteristics of ballistic motion are observable in transport experiments when the associated time scale is shorter than the impurity scattering time. We point out a general mechanism that circumvents this rule by linking different time scales through phase space volume conservation, a fundamental property of Hamiltonian systems. This finding was inspired by recent experiments on graphene antidot lattices, which show ballistic transport effects despite strong impurity scattering. We therefore exemplify this general mechanism for electronic transport in antidot superlattices and explain magnetoresistance experiments in graphene samples.

Electronic, but also photonic or phononic transport through a microscopic device is called *ballistic* when the *mean free path*  $\ell$  of the carriers exceeds the characteristic length scales of the device, or equivalently the *mean free time* becomes larger than the characteristic time scales of the intrinsic dynamics. In these cases transport is no longer dominated by diffusion due to e.g. impurity, phonon or electron-electron scattering. Instead ballistic transport is governed by external forces and the geometry of the device itself. In the ballistic transport regime details of the nonlinear dynamics of carriers can dominate the transport properties of the device, as was observed in various systems. Examples include quantum dots [1–5], ballistic cross junctions [6, 7], optical microcavities [8, 9] and microwave cavities [10].

We will show in this letter that counter-intuitively characteristics of ballistic motion may be observable in experiments, even if the mean free time (or *impurity scattering time*) is much shorter than the characteristic time scale of the ballistic nonlinear dynamics. This occurs simply as a consequence of phase space volume preservation in Hamiltonian systems. We will demonstrate this fundamental connection by studying transport through antidot superlattices (ADSLs), which are artificial crystals of repellers in high mobility two-dimensional electron gases (2DEGs). They are a prime example of a nanostructured material showing features of ballistic nonlinear dynamics. ADSLs were first fabricated into the 2DEG of AlGaAs/GaAs heterostructures [11–13] and since then realized in various materials [14–16] including graphene [17, 18] and very recently topological insulators [19].

The most prominent of a number of ballistic transport effects in antidot lattices is observed in their low temperature magnetoresistance  $R_{xx}$  at small magnetic fields (below the quantum Hall effect regime): it shows a series of pronounced peaks (Fig. 1). They have been observed in many different experimental realizations (e.g. [12, 13, 17–19]) and even in the fractional Quantum-Hall regime, when transport is carried by *composite fermions*, quasi-particles that experience a reduced effective magnetic field [20, 21].

It was observed by Weiss et al. [12] that these peaks occur at magnetic field values where collisionless cyclotron orbits can exist which encircle a certain number of antidots in the superlattice (cf. Fig. 2). They are therefore known as *commensurability peaks* (CPs). Soon it was understood, however, that the peaks are related to chaotic dynamics of electrons in ADSLs subject to a transverse magnetic field [22, 23]: the classical dynamics shows the generic *mixed phase space* structure of chaotic Hamiltonian systems [24, 25], where islands of *regular* (periodic and quasiperiodic) *motion* are embedded in a *chaotic sea* of irregular dynamics. The regular islands are also referred to as *nonlinear resonances* [24, 25]. In ADSLs the regular orbits can be either (permanently) “pinned” or “skipping” (see Fig. 2). Chaotic orbits can get *trapped* transiently by the fractal phase space structure near the islands mimicking the regular behavior for algebraically long times (for details see [26–28]). This leads to long time correlations in the chaotic dynamics and was made responsible for the occurrence of CPs in ADSLs due the presence of nonlinear resonances [22, 29–31].

How trapping of chaotic orbits leads to the observed resistance peaks, however, has remained controversial, as different research groups were emphasizing on different kind of orbits (pinned or skipping) [22, 29–31]. Nevertheless, the peaks were generally assumed to be washed out, when the mean scattering time becomes smaller than the corresponding characteristic time scale of the ballistic motion. Recent experiments by Sandner *et al.* [17] and Yagi *et al.* [18] on antidot lattices in monolayer graphene led us to question this, as the scattering time in these experiments is shorter than the typical period of the nonlinear resonances and therefore much too short to resolve the fine structures of the fractal phase space.

Why do the experiments exhibit CPs nevertheless? We will show that the resistance peaks survive the impact of these short impurity scattering times, as well as other kinds of disorder effects, because the fast chaotic time scale, the mean time between (successive) collisions of the electron trajectories with the antidots, is reduced by the mere existence of regular islands. Our analysis gives a simple and very general explanation of the phenomenon and will therefore be applicable to a wide range of systems with Hamiltonian ballistic dynamics where an intrinsic timescale (here the collision time with the anti-

\* george.datsaris@ds.mpg.de

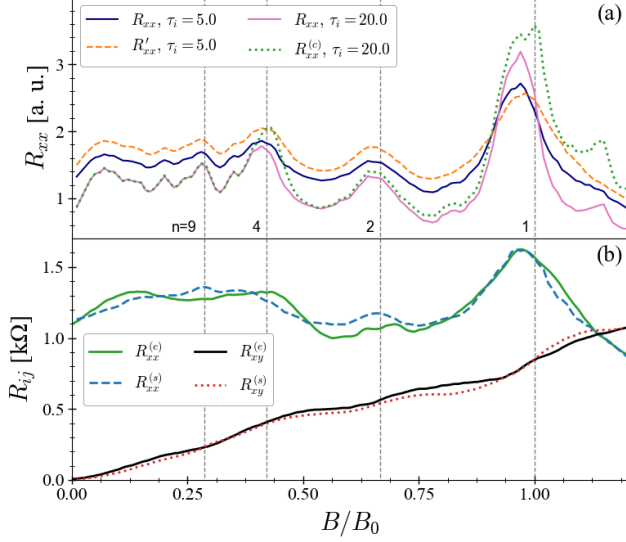


FIG. 1. (a): Magnetoresistivity simulations of antidot superlattices (ADSLs) demonstrating commensurability peaks ( $c = 0.1, d_0 = 0.3, \tau_i = 5, 20$ ).  $R'_{xx}$  denotes simulations with boundary roughness with parameter  $\varepsilon = 0.1$  (see Fig. 2b and the supplement for mathematical details).  $R^{(c)}_{xx}$  is the resistivity of the chaotic part of the phase space. Vertical dashed lines indicate the commensurable fields  $B_n$  (cf. Fig. 2). (b) Comparison of recent experiments of magneto- and Hall resistance  $R^{(e)}$  by Sandner *et al.* [17] with simulations  $R^{(s)}$  using parameters  $c = 0.2, d_0 = 0.3, \tau_i = 2.5$  and  $B_0 = 3.7$  T (the prefactor was determined by a least squares fit).

dots) of the chaotic trajectories is varied simply by varying the accessible phase space volume through a change in an external parameter (here the magnetic field). Furthermore, we are also able to resolve the long-standing controversy on the origin of the CPs by showing that they are caused by purely chaotic orbits.

We study the electron transport in the single particle picture at low but not ultracold temperatures when the coherence length of the carriers is much shorter than the elastic mean free path and the dynamics is well described by (quasi-)classical Hamiltonian dynamics [32]. We therefore model the carriers by a quasi-classical microcanonical ensemble at the Fermi energy  $E_F$ . The Hamiltonian is composed of a kinetic and potential energy part,  $\mathcal{H} = \mathcal{K}(p_x, p_y) + \mathcal{U}(x, y)$ , where  $\mathcal{K} = v_F \sqrt{p_x^2 + p_y^2}$  follows from the Dirac approximation of the dynamics of electrons in graphene with Fermi velocity  $v_F$  [33]. Our results apply equally well to the more common quadratic dispersion relation  $\mathcal{K} \propto \mathbf{p}^2$ . The magnetic field perpendicular to the graphene layer is introduced by *minimal coupling*,  $\mathbf{p} \rightarrow \mathbf{p} - q\mathbf{A}$ , choosing the symmetric gauge  $\mathbf{A} = -\frac{1}{2}\mathbf{r} \times \mathbf{B} = \frac{1}{2}(-yB, xB, 0)$ . We model the antidot super-lattice by a square array of localized, isotropic potential peaks of the form  $U = (E_F/c^4) [d_0/2 + c - r]^4$  if  $r = \sqrt{(x - x_a)^2 + (y - y_a)^2} < d_0/2 + c$  and 0 other-

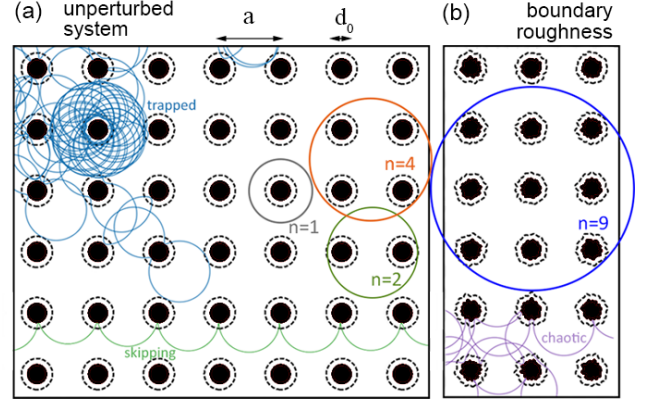


FIG. 2. Contours of the potential  $U$  (filled:  $U \geq 1$ , dashed:  $U = 0$ ). Antidots with boundary roughness are shown in (b), with parameter  $\varepsilon = 0.1$  (see supplement). Examples of chaotic, skipping, as well as *trapped* orbits at  $B = 1.0$  and pinned orbits enclosing  $n = 1, 2, 4$  and 9 antidots at the commensurable fields  $B_n \in \{1, 0.66, 0.42, 0.285\}$  are also shown.

wise.  $(x_a, y_a)$  is the center of the nearest antidot,  $d_0$  is the antidot diameter and  $c$  is a steepness controlling parameter. A contour plot of  $\mathcal{U}$ , which is the sum of all  $U$  for different antidot centers, is given in Fig. 2a. We add boundary roughness to the above potential by introducing fluctuating angle dependent antidot diameters  $d(\phi)$  with  $\langle d(\phi) \rangle_\phi = d_0$  (modeling antidot fabrication defects) as shown in Fig. 2b. In the supplement we discuss in more detail how we add boundary roughness and how we solve our model numerically.

Introducing dimensionless variables  $x_i \rightarrow x_i/a$  (where  $a$  is the antidot lattice spacing),  $v_i \rightarrow v_i/v_F$  and scaling the energy by the Fermi energy  $E_F = \hbar v_F \sqrt{\pi n_e}$  [33] ( $\approx 0.1 - 1$  eV for the electron densities  $n_e$  reported in [17]), the Hamiltonian of our model becomes

$$\mathcal{H} = \sqrt{(p_x + yB)^2 + (p_y - xB)^2} + \mathcal{U}(x, y). \quad (1)$$

In the following we study the dynamics on the manifold  $H = 1$  (i.e. the Fermi energy). We scale the magnetic field by its value at the principal ( $n = 1$ ) commensurability  $B_0 = 2\hbar\sqrt{\pi n_e}/(ea)$ , corresponding to a cyclotron diameter equal to the antidot lattice constant  $a$ . All times are given in units of  $t_0 = a/v_F$  and the cyclotron frequency is  $\omega_c = 2B$ .

From eq. (12) one can obtain the velocity timeseries (see supplement for the equations of motion and code used to simulate them). We then calculate the conductivities and resistivities using the Kubo formalism [34]. Following [22] we write

$$\sigma_{ij} \sim \int_0^\infty e^{-t/\tau_i} \langle v_i(t)v_j(0) \rangle_{E_F} dt, \quad (2)$$

$$R_{ij} = \frac{\sigma_{ij}}{\sigma_{xx}^2 + \sigma_{xy}^2} \quad (3)$$

with the conductivities  $\sigma_{ij}$  ( $ij = xx$  or  $xy$ ) and the magneto- and Hall-resistivity  $R_{xx}$  and  $R_{xy}$ , respectively (modulo some geometry prefactor).  $C_{ij}(t) \equiv \langle v_i(t)v_j(0) \rangle_{E_F}$  is the velocity correlation function (VCF), averaged over the initial conditions at the Fermi energy. Impurity scattering is introduced in Eq. 2 by assuming that the electron velocities are decorrelated by random scattering events which follow a Poisson distribution with mean time  $\tau_i$  [22]. In the experiments, the authors estimated  $\tau_i \approx 3.5$  [17].

In the following discussion it is advantageous to divide the VCFs into contributions of the different regions of the mixed phase space: the decaying correlations  $C_{ij}^{(c)}$  of the ergodic chaotic sea with relative phase space measure  $g_c$  and the non-decaying correlations  $C_{ij}^{(r)}$  of the regular islands with total relative measure  $g_r$ , where  $g_c + g_r = 1$ . We thus write  $C_{ij} = (1 - g_c)C_{ij}^{(r)} + g_c C_{ij}^{(c)}$ , and subsequently

$$\sigma_{ij} = (1 - g_c)\sigma_{ij}^{(r)} + g_c \sigma_{ij}^{(c)}. \quad (4)$$

Note that the regular islands of pinned orbits (see Fig. 2) correspond to almost circular (quasi-)periodic orbits, which in a smooth antidot potential are stable against the application of an external electric field [22]. Examples of these pinned orbits at the first four commensurabilities are shown in Fig. 2. Islands can also correspond to various forms of skipping [29] orbits, an example is also shown in the figure. It has been argued that skipping orbits are essential for the creation of resistance peaks [29–31, 35]. *Boundary roughness*, which probably is present in the experiments of Ref. [17], however, almost completely eliminates their existence without affecting the pinned orbits much.

Figure 1a shows example magnetoresistivity curves for the unperturbed antidot lattice for two values of the impurity scattering time  $\tau_i = 5, 20$ . An excellent fit to the experiment in magneto- and Hall resistivity is achieved for a small scattering time  $\tau_i = 2.5$ , as shown in Fig. 1b. As  $\omega_c \tau_i < 2\pi$  in the experiments, we cannot assume that the regular orbits are actually pinned (with  $\sigma_{ij}^{(r)} = 0$  as in Ref. [22]), since they get scattered before they close. We therefore treated them within the Kubo formalism. They lead to Drude like contributions with  $C_{xx}^{(r)}(t) \approx \cos(2Bt)/2$  and  $C_{xy}^{(r)}(t) \approx \sin(2Bt)/2$ .

The magnetoresistivity of an antidot lattice with boundary roughness ( $R'_{xx}$ ), shown in Fig. 1a exhibits surprisingly little differences from the unperturbed lattice. This suggests that the skipping orbits have little impact on the CPs. Furthermore, the resistivity curve  $R_{xx}^{(c)}$  of only the chaotic part of phase space, already fully reveals all CPs. It thus suffices to understand how the chaotic correlations change with the magnetic field to produce CPs.

Chaotic orbits get *trapped* near regular islands [22, 36, 37], i.e. they follow the quasiperiodic motion of the regular orbits for long times, as illustrated in Fig. 2a. This leads to long-time tails in the correlations of the chaotic

orbits. It was therefore argued that they would give rise to valleys rather than peaks in the magnetoresistivity [35]. We will show, however, that this effect is overcompensated by an initially accelerated correlation decay as a direct consequence of phase space volume conservation.

To do so, let us first inspect examples of the chaotic VCFs  $C_{ij}^{(c)}(t)$  in Fig. 3. In the absence of regular islands in phase space ( $B = 0.32$ ) we observe a single, fast correlation decay. In the presence of islands ( $B = 0.44$ ), we see long time tails in the correlations, originating from trapping. From fig. 3b, showing the envelope of the autocorrelation, however, it becomes clear, that the decay is an overlap of a fast and a slow component. We may think of it in the form

$$C_{xx}^{(c)}(t) \approx g_{\text{col}} C_{\text{fast}}(t) + g_{\text{trap}} C_{\text{slow}}(t) \quad (5)$$

(and similarly for the cross-correlation  $C_{xy}$ ) where  $g_{\text{trap}}$  is an appropriate measure of the trapping regions in the chaotic sea, and  $g_{\text{col}} = g_c - g_{\text{trap}}$  is its complement, i.e. the phase space region with strong chaotic scattering at the antidots (“*collisions*”). The black line of Fig. 3b illustrates this division by assuming exponential correlation decays with a fast and a slow time constant,  $\tau_{\text{fast}} = 3$  and  $\tau_{\text{slow}} = 350$ , with  $g_{\text{trap}} = 1.5\%$ . At this point, the detailed values are of no concern. What we see is that  $\tau_{\text{slow}}$  is orders of magnitude larger than  $\tau_i$ . The slow decay rate is therefore almost zero in comparison and the portion of trapped chaotic orbits is just a small correction to the portion of pinned orbits. The main contribution to the CPs stems from the change in the fast decay, which reflects the dynamics of the highly chaotic part of the phase space, a finding which is also reported by recent quantum simulations on graphene antidots by Power *et al.* [38]. This fast decay can be studied best in a billiard model with infinitely steep antidot walls, like in the Sinai billiard [39], which should be a good approximation for these highly chaotic trajectories.

In the remainder of this letter we will therefore study the periodic *Sinai billiard* (PSB), also known as *periodic Lorentz gas*, which is probably the most prominent example of a low-dimensional ergodic system [12, 39]. We simulate the PSB using an open source software we developed [40]. We denote the collision times in the PSB by  $t_\kappa$  and the mean collision time by  $\kappa$ , having in mind that the time scale of the fast correlation decay  $\tau_{\text{fast}}$  in the original model is approximated by  $\kappa$ .

Figure 4a shows  $\kappa$  as a function of the magnetic field. Remarkably, it exhibits pronounced valleys at the magnetic field values of the CPs in  $R_{xx}$  as shown in Fig. 4b for the billiard model. In the whole  $B$  range  $\kappa$  is comparable with  $\tau_i$  and even smaller at the commensurable fields. The valleys in  $\kappa(B)$  are the origin of the CPs. It is intuitive that more frequent collisions lead to reduced conductivity and thus increased  $R_{xx}$ , and we will further confirm this argument below using a simplified stochastic model. But first we show that the structure of  $\kappa(B)$  has a deep connection with the mixed nature of the phase

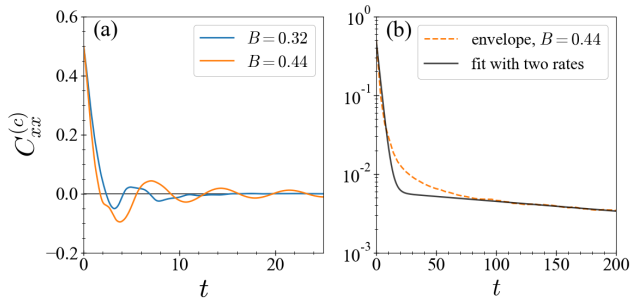


FIG. 3. Velocity correlation function of chaotic orbits for  $B = 0.32, 0.44$  and  $c = 0.2, d_0 = 0.3$ . While for non-commensurate magnetic fields ( $B = 0.32$ ) it shows a fast exponential decay, for commensurate magnetic fields ( $B = 0.44$ ) it exhibits an additional slow decay as seen in the envelope (dashed line, panel b).

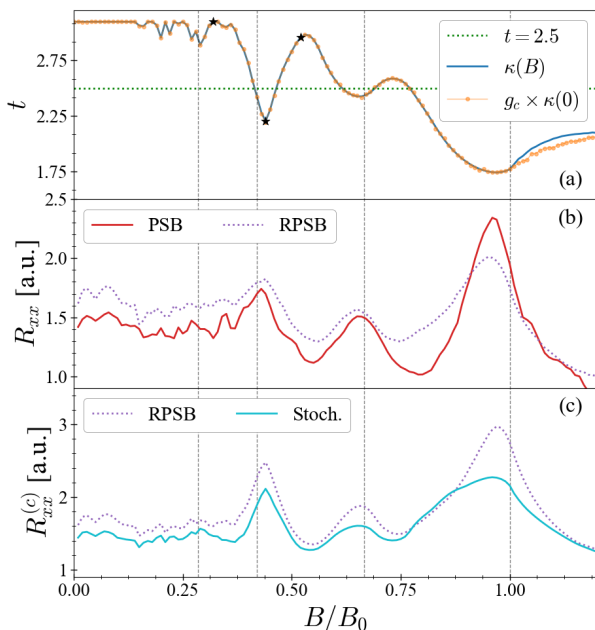


FIG. 4. (a): Average collision time  $\kappa$  in the periodic Sinai billiard (PSB) versus  $B$ . It coincides with the portion of chaotic orbits  $g_c$  times  $\kappa(0)$ . (b) The resistivity curve of the random PSB (RPSB) does not differ much from that of the PSB. (c) The RPSB resistivity curve is approximated sufficiently well by the stochastic model (labeled “Stoc.”). All curves are calculated with  $\tau_i = 5.0, d_0 = 0.3$ .

space: Fig. 4a indeed shows that it is directly proportional to the portion of the chaotic part of phase space  $g_c(B)$ .

We can understand this striking fact using *Kac’s lemma* [41–44], which is a direct consequence of phase space volume conservation in Hamiltonian systems. We obtain a map of the flow  $\Phi^t$  by discretizing in time,  $f := \Phi^{\Delta t_\varepsilon}$ , with  $\Delta t_\varepsilon \sim \varepsilon$ . Kac’s lemma states that the mean number of iterations  $\langle N_S \rangle$  needed to return to a

compact subset  $\mathcal{S}$  of the phase space  $\mathcal{M}$  is given by

$$\langle N_S \rangle(B) = \frac{\mu(\mathcal{M}_{acc}; B)}{\mu(\mathcal{S}; B)}, \quad (6)$$

where  $\mu(\cdot)$  is the phase space measure and  $\mathcal{M}_{acc}$  the part of the phase space accessible to orbits starting in  $\mathcal{S}$ . Let  $\mathcal{T}_S(B) = \Delta t_\varepsilon \times \langle N_S \rangle(B)$  denote physical time instead of map iterations. Let  $\mathcal{W}$  be a circle of radius  $d_0/2 + \varepsilon$  concentric to the antidot and define  $\mathcal{S}_\varepsilon \subset \mathcal{M}$  such that

$$\mathcal{S}_\varepsilon = \{\vec{x}, \vec{v} : \vec{x} \in \mathcal{W} \text{ and } \vec{v} \cdot \vec{\eta}(\vec{x}) < 0\} \quad (7)$$

where  $\vec{\eta}(\vec{x})$  is the vector normal to  $\mathcal{W}$ . The mean collision time  $\kappa$  of the PBS is exactly  $\mathcal{T}_S$  in the limit  $\varepsilon \rightarrow 0$ .

To find  $\mu(\mathcal{S}; B)$  we first realize that it does not depend on the magnetic field, i.e.  $\mu(\mathcal{S}; B) = \mu(\mathcal{S}; 0) = \mu(\mathcal{S})$ . Then, using (6) at  $B = 0$ , we have

$$\mathcal{T}_S(0) = \left( \frac{\Delta t_\varepsilon}{\mu(\mathcal{S}_\varepsilon)} \right) \mu(\mathcal{M}_{acc}; 0) = \left( \frac{\Delta t_\varepsilon}{\mu(\mathcal{S}_\varepsilon)} \right), \quad (8)$$

because the PSB without magnetic field is fully ergodic and thus  $\mu(\mathcal{M}_{acc}; 0) = \mu(\mathcal{M}) = 1$ . By substitution we get  $\mathcal{T}_S(B) = \mu(\mathcal{M}_{acc}; B) \times \mathcal{T}_S(0)$ . For small enough magnetic fields all chaotic orbits (and up to measure 0 only those) collide with the antidots. In the limit  $\varepsilon \rightarrow 0$  both  $\Delta t_\varepsilon$  and  $\mu(\mathcal{S}_\varepsilon)$  go to 0 linearly with  $\varepsilon$ , therefore their ratio converges, i.e.  $\mathcal{T}_S \rightarrow \kappa$ . Since by definition  $\mu(\mathcal{M}_{acc}) = g_c$ , we find that the mean collision time is given by the fraction of chaotic orbits as a function of the magnetic field  $B$ , times the mean collision time at  $B = 0$

$$\kappa(B) = g_c(B) \times \kappa(0). \quad (9)$$

From this derivation it becomes also clear that the collision times are not sensitive to boundary roughness. This is intuitive, since the dynamics is already highly chaotic. To confirm this we also simulated a “rough” Sinai billiard where the particle gets reflected in a random angle at collision with the antidot (RPSB), corresponding to strong boundary roughness. The changes in the magnetoresistivity are only small indeed as shown in Fig. 4b.

For completeness we now conclude our argumentation by linking the collision times to the resistivities in a simplified purely stochastic model for the motion in the billiard with boundary roughness (RPSB). Since this is not crucial for the understanding of the main message of our paper we only present a summary here and give more details in the supplement. We approximate the dynamics by a renewal process of stochastic collision events and free cyclotron motion in-between collisions. The only input into the stochastic model is the distribution of times in between collisions, which is obtained from the PSB.

Our stochastic model reproduces the contribution of the chaotic orbits to the CPs in the RPBS in very good approximation, as shown in Fig. 4c. This confirms our

claim that the CPs are due merely to the distribution of collision times in the antidot lattice.

In conclusion, we have explained recent magnetotransport experiments on graphene antidot lattices using appropriate quasiclassical electron dynamics. By this we solved a decades old riddle on the influence of nonlinear resonances on magnetotransport in antidot superlattices. Due to the fundamental nature of the mechanism linking the time scales, which only depends on the basic properties of chaotic Hamiltonian systems with mixed phase space, it will be generally applicable to a wide range of mesoscopic systems.

## SUPPLEMENTAL MATERIAL

The computer code we used to perform the simulations of this work is available online: [https://github.com/Datseris/arXiv\\_1711.05833](https://github.com/Datseris/arXiv_1711.05833).

### A. Boundary Roughness

As mentioned in the main text, we model the antidot super-lattice by a square array of localized potential peaks of the form

$$U_a = \left(\frac{E_F}{c^4}\right) \left[\frac{d_0}{2} + c - r_a\right]^4 \quad (10)$$

if  $r_a = \sqrt{(x - x_a)^2 + (y - y_a)^2} < \frac{d_0}{2} + c$  and 0 otherwise.  $(x_a, y_a) = (na, ma)$  with  $n, m \in \mathbb{N}$  is the center of the (nearest) antidot and  $a$  is the super-lattice constant.  $d_0$  is the antidot diameter (in the experiment by Sandner *et al.* [17] reported values are  $d_0 \approx 25 - 30\text{nm}$  with antidot spacing  $a \approx 100\text{nm}$ ). The parameter  $c$  defines a cut-off distance of the potential and it is also the parameter that controls the steepness of the antidots. The full potential is then the (infinite) sum of the above localized potentials over all antidot centers  $\mathcal{U} = \sum_{n,m} U_a$ . Numerically we do not have an infinite sum of potentials, but instead use the modulo operation of  $x, y$  with  $a$ .

We can add boundary roughness (which aims to model the antidot fabrication defects) to the above potential by making the antidot diameter depend pseudo-randomly on the position. Specifically, let  $\tilde{x} = x - x_a$ ,  $\tilde{y} = y - y_a$  and define  $\phi = \arctan(\tilde{y}/\tilde{x})$ . We can then write

$$d(\phi) = d_0 + d_0\varepsilon \sum_{\zeta=1}^M \nu(x_a, y_a, \zeta) \times \sin(\zeta\phi) \quad (11)$$

with  $\nu$  being random numbers uniformly distributed in  $[-0.5, 0.5]$  which are different for each combination of  $x_a, y_a, \zeta$ , so that on average  $\langle d(\phi) \rangle = d_0$ .  $M$  is the total number of sine modes used (measure of the edge complexity) and  $\varepsilon$  measures the relative boundary roughness. In the numerical computations we used an array of  $100 \times M$  random numbers repeated periodically and used  $M = 16$  for all simulations shown in the manuscript.

Note that the boundary roughness is distinct from the impurity scattering, which we also include in our model, see eq. (17).

A contour plot of  $\mathcal{U}$  is given in Fig. 1 of the manuscript. However, details of the potential form do not play an important role. Even though of course the diameter and smoothness of the antidots are important parameters, different functional forms (e.g.  $\mathcal{U} \propto [\cos(2\pi x/a) \cos(2\pi y/a)]^\beta$ , like in [22]) for the potential have very little impact on the resistivities, and no bearing at all on our main conclusions, as it becomes clear from our main manuscript. Equally, using a conical or a quadratic kinetic energy term (see main text) does not lead to any qualitative changes which we have tested numerically (not shown here). This is not surprising since all effects studied are also observable in the billiard model which uses hard-wall potentials for the antidots and is completely indifferent to the form of the kinetic energy (provided that it is isotropic).

### B. Equations of Motion

In the main manuscript we use a kinetic energy term of the form  $\mathcal{K} = v_F \sqrt{p_x^2 + p_y^2}$ . To evolve our system in time, we first introduce dimensionless variables  $x_i \rightarrow x_i/a$ ,  $v_i \rightarrow v_i/v_F$  and scale the energy by the Fermi energy  $E_F = \hbar v_F \sqrt{\pi n_e}$  ( $\approx 0.1 - 1$  eV for the electron densities  $n_e$  reported in [17]). In these units  $d_0$  is now an effective parameter that measures the ratio of the antidot diameter to the antidot spacing. We scale the magnetic field by its value at the principle commensurability  $B_0 = 2\hbar\sqrt{\pi n_e}/(ea)$ , corresponding to a cyclotron diameter equal to the antidot lattice constant  $a$ . Then, the Hamiltonian of our model becomes

$$\mathcal{H} = \sqrt{(p_x + yB)^2 + (p_y - xB)^2} + \mathcal{U}(x, y) \quad (12)$$

which is scaled such that it has numerical value of 1 (constant). All times are given in units of  $t_0 = a/v_F$  and the cyclotron frequency is  $\omega_c = 2B$ . Eq. (12) leads to the equations of motion  $\dot{\mathbf{x}} = \partial\mathcal{H}/\partial\mathbf{p}$ ,  $\dot{\mathbf{p}} = -\partial\mathcal{H}/\partial\mathbf{x}$ . We then obtain equations for velocities instead of momenta,

$$\dot{x} = v_x \quad (13)$$

$$\dot{y} = v_y \quad (14)$$

$$\dot{v}_x = v_y \left( \frac{v_x \frac{\partial\mathcal{U}}{\partial y} - v_y \frac{\partial\mathcal{U}}{\partial x} + 2B}{1 - \mathcal{U}} \right) \quad (15)$$

$$\dot{v}_y = -v_x \left( \frac{v_x \frac{\partial\mathcal{U}}{\partial y} - v_y \frac{\partial\mathcal{U}}{\partial x} + 2B}{1 - \mathcal{U}} \right). \quad (16)$$

Eqs. (13)-(16) describe (classical) hyper-relativistic particles in magnetic field  $B$  and potential  $\mathcal{U}$ , and are highly nonlinear and not analytically solvable. The velocity timeseries are obtained by numerical integration of the equations of motion using standard Runge-Kutta schemes.

### C. Impurity Scattering

After we have the velocity timeseries we use Fourier transforms and the Wiener-Khinchin theorem to numerically calculate the velocity correlation functions (VCFs) for each individual trajectory. We then proceed to calculate the conductivities using the Kubo formalism [34], following [22]

$$\sigma_{ij} \sim \int_0^\infty e^{-t/\tau_i} C_{ij}(t) dt \quad (17)$$

where  $C_{ij}(t) \equiv \langle v_i(t)v_j(0) \rangle_{E_F}$  is the (equilibrium) VCF which is averaged over available initial conditions at the Fermi energy  $E_F$ . Numerically we used 5000 uniformly distributed random initial conditions, evolved for 5000 units of time, and averaged the VCFs over those to obtain sufficient convergence for  $\sigma_{ij}$ . To calculate long time correlations in the absence of impurity scattering like those shown in Fig. 3 of the main text, we have used 10000 orbits for 10000 units of time.

Equation (17) includes modeling of random scattering by impurities by making two assumptions: first, after scattering by an impurity the electron velocity directions are fully randomized and therefore decorrelated. Second, impurity scattering events are Poisson distributed with characteristic time  $\tau_i$ . Under these assumptions it is straight-forward to show [22] that impurity scattering leads to an exponential suppression of the VCF by a factor  $e^{-t/\tau_i}$  [45].

### D. Stochastic Model

In this section of the supplemental material we want to derive the expressions for the velocity correlation functions (and thus the resistivities) of the simplified stochastic model for the dynamics in the rough periodic Sinai

billiard (RPSB) introduced in the manuscript. We approximate the dynamics by a renewal process of stochastic scattering events (the distribution of the scattering times reflects the geometry of the antidot lattice) and free cyclotron motion in between scattering events. Each scattering event with a rough boundary leads to a random change in the velocity angle

$$\alpha = \pi + 2\psi,$$

where  $\psi$  is the random angle formed by the normal of the boundary segment and the velocity vector of the trajectory undergoing the scattering event. Under the assumption that all spatial orientations of the boundary segments are equally probable the probability density of hitting a segment with angle  $\psi$  is

$$h(\psi) = \frac{1}{2} \cos \psi, \text{ with } \psi \in [-\pi/2, \pi/2]. \quad (18)$$

Notice that this stochastic model is not the same as the RPSB; in the latter there is a strong correlation between the reflected angle and the subsequent collision time. This correlation does not exist in the stochastic model, as well as any knowledge of phase space volumes.

The velocity correlation functions are

$$S_{xx} = \langle v_y(t)v_x(0) \rangle = v_0^2 \langle \cos(\varphi(t)) \cos(\varphi(0)) \rangle \quad (19)$$

$$S_{yx} = \langle v_y(t)v_x(0) \rangle = v_0^2 \langle \sin(\varphi(t)) \cos(\varphi(0)) \rangle, \quad (20)$$

where  $v_0$  is the constant absolute value of the velocity ( $v_0 = 1$  in our units) and the ensemble average  $\langle \cdot \rangle$  reduces to an average over the initial angle  $\varphi_0$  of the velocities and the collision events. In the free propagation in-between events the velocity angle changes by  $\Delta\varphi(t) = \omega\Delta t$ , where the cyclotron frequency  $\omega$  in our units is given by  $\omega = 2B$ . The contribution to the correlation functions of all trajectories that have scattered (exactly)  $m$  times up to time  $t$  is given by

$$S_{xx}(t|m) = P_m(t; B) \int_{-\pi}^{\pi} d\varphi_0 \int_{-\pi/2}^{\pi/2} d\psi_1 \cdots \int_{-\pi/2}^{\pi/2} d\psi_m \frac{\cos \varphi_0}{2\pi} \cos \left( \omega t + \varphi_0 + m\pi + 2 \sum_{i=1}^m \psi_i \right) \frac{\prod_{i=1}^m \cos \psi_i}{2^m} \quad (21)$$

$$S_{yx}(t|m) = P_m(t; B) \int_{-\pi}^{\pi} d\varphi_0 \int_{-\pi/2}^{\pi/2} d\psi_1 \cdots \int_{-\pi/2}^{\pi/2} d\psi_m \frac{\cos \varphi_0}{2\pi} \sin \left( \omega t + \varphi_0 + m\pi + 2 \sum_{i=1}^m \psi_i \right) \frac{\prod_{i=1}^m \cos \psi_i}{2^m}, \quad (22)$$

where  $P_m(t; B)$  is the probability that a trajectory has scattered exactly  $m$  times up to time  $t$ . The  $\psi_i$  integrals can be easily carried out successively. Using the notation  $\phi_m = \omega t + \varphi_0 + m\pi + 2 \sum_{i=1}^m \psi_i$ , we write

$$\begin{aligned} \cos(\phi_m) &= \cos(\phi_{m-1} + 2\psi_m + \pi) \\ &= -\cos(\phi_{m-1}) \cos(2\psi_m) + \sin(\phi_{m-1}) \sin(2\psi_m) \end{aligned}$$

and similarly

$$\sin(\phi_m) = -\cos(\phi_{m-1}) \sin(2\psi_m) - \sin(\phi_{m-1}) \cos(2\psi_m).$$

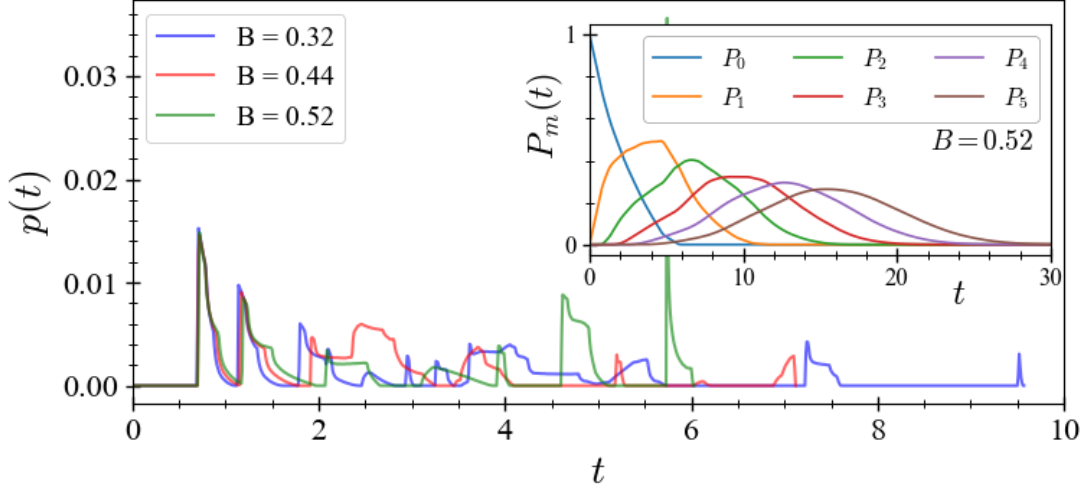


FIG. 5. Probability density function of the collision times  $p(t_n)$  in the rough periodic Sinai billiard for the magnetic fields values marked by black stars in Fig. 4 of the manuscript, i.e.  $B \in \{0.32, 0.44, 0.52\}$ . The inset shows numerically computed probabilities  $P_m(t; B)$  for  $B = 0.52$ .

With

$$\frac{1}{2} \int_{-\pi/2}^{\pi/2} \cos(x) \cos(2x) dx = \frac{1}{3},$$

$$\frac{1}{2} \int_{-\pi/2}^{\pi/2} \cos(x) \sin(2x) dx = 0$$

and

$$\frac{1}{2\pi} \int_{-\pi}^{\pi} \cos(\varphi_0) \cos(\omega t + \varphi_0) d\varphi_0 = \frac{1}{2} \cos(\omega t)$$

we find  $C_{xx}(t|m) = \frac{1}{2} \left(-\frac{1}{3}\right)^m \cos(\omega t)$  and  $C_{yx}(t|m) = \frac{1}{2} \left(-\frac{1}{3}\right)^m \sin(\omega t)$ . This finally allows us to write the correlation functions as the sum of these contributions:

$$S_{xx}(t) = \frac{1}{2} \sum_{m=0}^{\infty} \left(-\frac{1}{3}\right)^m P_m(t; B) \cos(\omega t) \quad (23)$$

$$S_{yx}(t) = \frac{1}{2} \sum_{m=0}^{\infty} \left(-\frac{1}{3}\right)^m P_m(t; B) \sin(\omega t). \quad (24)$$

The probability density function (pdf) of the collision time  $p(t)$  is a complicated function that is very sensitive to changes in the magnetic field, as shown in Fig. 5. Therefore it is hard to find a useful analytical model for the probability  $P_m(t; B)$ . Only in the limit of large  $m$  they are well approximated by Gaussians (see e.g. [46]). We are, however, mainly interested in short times and thus small  $m$ . Therefore we choose to calculate the  $P_m(t; B)$  numerically using the following method:

let  $q_m(t)$  denote the pdf for the  $m$ -th scattering event ( $m \geq 1$ ) occurring at time  $t$ . It can be calculated through recursive convolution with the pdf  $p(t)$ ,

$$q_m(t) = \int_0^t dz p(z) q_{m-1}(t-z)$$

with  $q_1(t) \equiv p(t)$ . Then  $P_m(t)$  can be found from  $q_m$  using the survival function  $W(t) = \int_t^{\infty} p(t') dt'$

$$P_m(t) = \int_0^t dz W(z) q_m(t-z) \quad (25)$$

for  $m > 0$  and  $P_0(t) \equiv W(t)$ . Examples of  $P_m(t)$  are shown in the inset of Fig. 5. Finally, using the Kubo-formula (Eq. 2 and 3 of the manuscript) with impurity scattering time  $\tau_i = 5$  we obtain the magnetoresistance curve shown in Fig. 4 of the manuscript, which clearly demonstrates that the main contribution to the commensurability peaks is already captured by this simple model.

## ACKNOWLEDGMENTS

We thank Andreas Sandner and Jonathan Eroms very much for granting us access to their experimental data and fruitful discussions. We thank Stephan Eule for helpful discussions.

- 
- [1] C. M. Marcus, A. J. Rimberg, R. M. Westervelt, P. F. Hopkins, and A. C. Gossard, *Physical Review Letters* **69**, 506 (1992).
- [2] R. Ketzmerick, *Physical Review B* **54**, 10841 (1996).
- [3] A. P. Micolich, R. P. Taylor, A. G. Davies, J. P. Bird, R. Newbury, T. M. Fromhold, A. Ehlert, H. Linke, L. D. Macks, W. R. Tribe, E. H. Linfield, D. A. Ritchie, J. Cooper, Y. Aoyagi, and P. B. Wilkinson, *Physical Review Letters* **87** (2001), 10.1103/physrevlett.87.036802.
- [4] H. Hennig, R. Fleischmann, L. Hufnagel, and T. Geisel, *Physical Review E* **76** (2007), 10.1103/physreve.76.015202.
- [5] L. A. Ponomarenko, F. Schedin, M. I. Katsnelson, R. Yang, E. W. Hill, K. S. Novoselov, and A. K. Geim, *Science* **320**, 356 (2008).
- [6] T. Geisel, R. Ketzmerick, and O. Schedletzky, *Physical Review Letters* **69**, 1680 (1992).
- [7] H. U. Baranger and R. M. Westervelt, in *Nanotechnology* (Springer, New York, NY, 1999) pp. 537–628.
- [8] J. U. Nöckel and A. D. Stone, *Nature* **385**, 45 (1997).
- [9] H. Cao and J. Wiersig, *Rev. Mod. Phys.* **87**, 61 (2015).
- [10] S. Gehler, S. Löck, S. Shinohara, A. Bäcker, R. Ketzmerick, U. Kuhl, and H.-J. Stöckmann, *Physical Review Letters* **115** (2015), 10.1103/physrevlett.115.104101.
- [11] K. Ensslin and P. M. Petroff, *Phys. Rev. B* **41**, 12307 (1990).
- [12] D. Weiss, M. L. Roukes, A. Menschig, P. Grambow, K. von Klitzing, and G. Weimann, *Phys. Rev. Lett.* **66**, 2790 (1991).
- [13] A. Lorke, J. P. Kotthaus, and K. Ploog, *Phys. Rev. B* **44**, 3447 (1991).
- [14] Z. L. Xiao, C. Y. Han, U. Welp, H. H. Wang, V. K. Vlasko-Vlasov, W. K. Kwok, D. J. Miller, J. M. Hiller, R. E. Cook, G. A. Willing, and G. W. Crabtree, *Applied Physics Letters* **81**, 2869 (2002).
- [15] R. Wördenweber, P. Dymashevski, and V. R. Misko, *Physical Review B* **69**, 184504 (2004).
- [16] S. Neusser, B. Botters, and D. Grundler, *Physical Review B* **78**, 054406 (2008).
- [17] A. Sandner, T. Preis, C. Schell, P. Giudici, K. Watanabe, T. Taniguchi, D. Weiss, and J. Eroms, *Nano Lett.* **15**, 8402 (2015).
- [18] R. Yagi, R. Sakakibara, R. Ebisuoka, J. Onishi, K. Watanabe, T. Taniguchi, and Y. Iye, *Phys. Rev. B* (2015).
- [19] H. Maier, J. Ziegler, R. Fischer, D. Kozlov, Z. D. Kvon, N. Mikhailov, S. A. Dvoretzky, and D. Weiss, *Nature Communications* **8**, 1 (2017), arXiv:1708.07766.
- [20] W. Kang, H. L. Stormer, L. N. Pfeiffer, K. W. Baldwin, and K. W. West, *Physica B* **211**, 396 (1995).
- [21] R. Fleischmann, T. Geisel, C. Holzknacht, and R. Ketzmerick, *Europhys. Lett.* **36**, 167 (1996).
- [22] R. Fleischmann, T. Geisel, and R. Ketzmerick, *Phys. Rev. Lett.* **68**, 1367 (1992).
- [23] E. Vasiliadou, R. Fleischmann, D. Weiss, D. Heitmann, K. V. Klitzing, T. Geisel, R. Bergmann, H. Schweizer, and C. T. Foxon, *Physical Review B* **52**, R8658 (1995).
- [24] R. Mackay, J. Meiss, and I. Percival, *Physica D: Nonlinear Phenomena* **13**, 55 (1984).
- [25] A. Lichtenberg and M. Lieberman, *Regular and Chaotic Dynamics (Applied Mathematical Sciences)* (Springer, 2010).
- [26] J. D. Meiss and E. Ott, *Physical Review Letters* **55**, 2741 (1985).
- [27] T. Geisel, A. Zacherl, and G. Radons, *Physical Review Letters* **59**, 2503 (1987).
- [28] T. Geisel, A. Zacherl, and G. Radons, *Zeitschrift für Physik B Condensed Matter* **71**, 117 (1988).
- [29] É. Baskin, G. Gusev, Z. Kvon, A. Pogosov, and M. Entin, *JETP Lett.* **55**, 678 (1992).
- [30] R. Schuster, G. Ernst, K. Ensslin, M. Entin, M. Holland, G. Böhm, and W. Klein, *Phys. Rev. B* **50**, 8090 (1994).
- [31] S. Ishizaka and T. Ando, *Phys. Rev. B* **55**, 16331 (1997).
- [32] K. Richter, *Europhys. Lett.* **29**, 7 (1995).
- [33] a. H. Castro Neto, F. Guinea, N. M. R. Peres, K. S. Novoselov, and a. K. Geim, *Reviews of Modern Physics* **81**, 109 (2009), arXiv:0709.1163.
- [34] R. Kubo, *J. Phys. Soc. Jpn.* **12**, 570 (1957).
- [35] M. Fließner, G. J. O. Schmidt, and H. Spohn, *Phys. Rev. E* **53**, 5690 (1996).
- [36] M. Tabor, *Chaos and Integrability in Nonlinear Dynamics* (Wiley, 1989) p. 384.
- [37] V. I. Arnold, *Mathematical Methods of Classical Mechanics*, Graduate Texts in Mathematics, Vol. 60 (Springer New York, New York, NY, 1989).
- [38] S. R. Power, M. R. Thomsen, A. P. Jauho, and T. G. Pedersen, *Physical Review B* **96** (2017), 10.1103/PhysRevB.96.075425, arXiv:arXiv:1703.05665v2.
- [39] Y. G. Sinai, *Russ. Math. Surv.* **25**, 137 (1970).
- [40] G. Datsaris, *The Journal of Open Source Software* **2**, 458 (2017).
- [41] M. Kac, *Bull. Amer. Math. Soc* **20**, 376 (1947).
- [42] R. S. MacKay, *Journal of Nonlinear Science* **4**, 329 (1994).
- [43] J. D. Meiss, *Chaos* **7**, 139 (1997).
- [44] E. G. Altmann and T. Tel, *Phys. Rev. Lett.* **100**, 1 (2008).
- [45] We have numerically confirmed that including stochastic scattering events in the dynamics gives the same result as the exponential dampening of eq. (17), even in the case of small angle scattering, where  $\tau_i$  has to be regarded as the *transport mean free time*.
- [46] K. V. Mitov and E. Omev, *Renewal Processes* (Springer International Publishing, 2014).